

INTEGRITY FACTORS OF THE BASINS OF ATTRACTION OF AN AXIALLY EXCITED CYLINDRICAL SHELL

Frederico M. A. Silva^{a,b}, Augusta F. Brazão^{a,c}, Zenón J. G. N. Del Prado^{a,d}, Paulo B. Gonçalves^e

^a*School of Civil Engineering, Federal University of Goiás, Av. Universitária, 74605-220, Goiânia-Goiás, Brazil,* ^b*silvafma@eec.ufg.br,* ^c*augustafb@hotmail.com,* ^d*zenon@eec.ufg.br.*

^e*Civil Engineering Department, Pontifical Catholic University, 22451-900, Rio de Janeiro-RJ, Brazil, paulo@puc-rio.br*

Keywords: Cylindrical shells, integrity factor, basins of attraction, nonlinear analysis.

Abstract. The aim of this investigation is to analyze the integrity factors of the basins of attraction of cylindrical shells subjected to an axial load composed of a static pre-load plus a harmonic excitation. The shell is described by the Donnell nonlinear shallow shell theory. The lateral displacement field is approximated qualitatively by a modal expansion with two degrees of freedom, containing the basic vibration mode plus an axi-symmetric mode with twice the number of waves as the basic mode, thus describing consistently the asymmetry of the nonlinear displacement field of the cylindrical shell surface. The discretized nonlinear differential equations of motion are obtained by the Galerkin method. In this paper special attention is paid to the influence of static pre-loading on the integrity of the basins of attraction of the permanent response of the harmonically excited cylindrical shell. For this, we obtain the parametric instability and permanent escape boundaries in the force control space, the bifurcation diagrams in both the pre- and post-buckling wells and the evolution of the basins of attraction for increasing levels of static pre-load. From this parametric analysis the variation of the integrity factor with the applied load is analyzed. It is shown that the variation of the integrity factor of each basin of attraction provides the designer with essential information on the safety of each stable long term solution of the excited shell

1 INTRODUCTION

Cylindrical shells have several applications in different engineering areas such as aeronautics, offshore, mechanics and civil engineering. In civil engineering, cylindrical shells can be found in reservoirs, silos and roofs. Even with a simple geometry, cylindrical shells can display very complex non-linear behavior when subjected to external excitations.

Recently, for systems with multiple potential wells, or multiple attractors, the use of basins of attraction has been proposed as a tool to evaluate the degree of safety of a structure when subjected to external loads (Gonçalves et al., 2007a, b). For that, an initial interest region in the phase space is defined, the existing attractors are identified and the evolution of the basins of attraction associated to a control parameter is studied. Particular importance is given to the size and continuity of the basin of attraction (Rega e Lenci, 2005; Silva, 2008; Gonçalves et al. 2010) and to the boundary structure, which can be continuous or fractal. The basic concepts used in this work can be found in Thompson (1989), Soliman e Thompson (1989, 1991), Thompson e Soliman (1991), Lansbury et al. (1992) and Soliman (1993). Important contributions to the evolution of basins of attraction can be also found in McDonald et al. (1985) and Grebogi et al. (1987).

In this work, for a simply supported cylindrical subjected to increasing levels of harmonic axial load, the integrity of solutions contained in the pre-buckling potential well and how they are limited by the post-buckling small amplitude and large cross-well motions is studied to evaluate the changes in the integrity factor and, consequently, on the structure safety level.

2 PROBLEM FORMULATION

Consider a perfect simply supported circular cylindrical shell with length L , radius R and thickness h . It is supposed that the Shell is made of an elastic isotropic homogeneous material with Young modulus E , Poisson ratio ν and density ρ . The axial, circumferential and radial coordinates are given by x , θ and z respectively and the field displacements are u , v e w as seen in Figure 1.

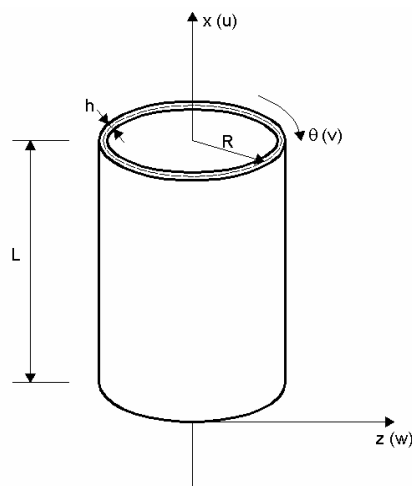


Figure1: Shell geometry and system coordinates

The shell is subjected to a uniformly distributed axial load applied on both ends, $x = 0, L$, and given by:

$$P(t) = P_0 + P_1 \cos(\omega t) \quad (1)$$

where P_0 is the static load component; P_1 is the amplitude of the harmonic load component; t

the time and ω is the frequency of excitation.

Using the Donnell shallow shell theory, the non-linear dynamic equilibrium equation and compatibility equation are given by:

$$\begin{aligned} \rho h R^2 \ddot{w} - D \nabla^4 w - R f_{,xx} + (f_{,\theta\theta} w_{,xx} - 2f_{,x\theta} w_{,x\theta} + f_{,xx} w_{,\theta\theta}) \\ + 2\eta_1 \rho h \omega_0^2 \dot{w} + \eta_2 D \nabla^4 \dot{w} = 0 \end{aligned} \quad (2)$$

$$\frac{1}{Eh} \nabla^4 f = -\frac{1}{R} w_{,xx} - w_{,xx} w_{,yy} + w_{,xy}^2 \quad (3)$$

where

$$f = f_p + f_h \quad f_p = -\frac{1}{2} P_0 \theta^2 \quad (4)$$

with ∇^4 is the Cartesian bi-harmonic operator; η_1 and η_2 are the viscous and material damping coefficients, respectively, ω_0 is the natural frequency of the shell, f the Airy stress function and D is the shell bending stiffness factor given by:

$$D = Eh^3/12(1-\nu^2) \quad (5)$$

In this work, the following non-dimensional parameters are used:

$$\begin{aligned} W = \frac{w}{h} \quad \zeta = \frac{x}{L} \quad \theta = \frac{y}{R} \quad \tau = \omega_0 t \\ \alpha = \frac{h}{R} \quad \beta = \frac{h}{L} \quad \gamma = \frac{nL}{\pi R} \quad \bar{f} = \frac{R}{Eh^2 L^2} f \\ \Gamma_0 = \frac{P_0}{P_{cr}} = \frac{R\sqrt{3(1-\nu^2)}}{Eh^2} P_0 \quad \Gamma_1 = \frac{P_1}{P_{cr}} = \frac{R\sqrt{3(1-\nu^2)}}{Eh^2} P_1 \end{aligned} \quad (6)$$

To obtain a consistent modeling with a limited number of modes, the sum of shape functions for the displacements must express the inherent non-linear coupling among these modes and the in-out asymmetry of the deformed curved shell surface. Perturbation methods may be used to identify these essential modes and the importance of each mode in the modal expansion can be quantified by computing the contribution of each mode to the total energy of the system (Gonçalves et al. 2008).

One must consider at least two modes to obtain a qualitatively correct description of the non-linear vibration modes, namely the basic vibration mode and the corresponding axisymmetric mode with twice the number of half waves in the axial direction as the basic mode, that is:

$$W = \xi(\tau)_{11} \cos(n\theta) \sin(m\pi\zeta) + \xi(\tau)_{02} \cos(2m\pi\zeta) \quad (7)$$

where n is the circumferential wavenumber and m is the longitudinal half-wave number.

Substituting Eq. (7) on the right hand side of Eq. (3) it is possible to obtain the homogeneous part of the stress function f which, in non-dimensional form, is given by:

$$\begin{aligned}
\bar{f} = & -\frac{1}{4} \frac{\beta^2}{\alpha^2} \frac{\theta^2}{\pi \sqrt{3(1-\nu^2)}} \left[\Gamma_0 + \Gamma_1 \cos(\Omega \tau) \right] + \frac{m^2}{\pi^2 (m^2 + \gamma^2)^2} \xi_{11}(\tau) \cos(n\theta) \sin(m\pi \zeta) \\
& + \frac{1}{4} \frac{\xi_{02}(\tau)}{m^2 \pi^2} \cos(2m\pi \zeta) + 2 \frac{\alpha m^2 n^2}{\pi^2 (m^2 + \gamma^2)^2} \xi_{11}(\tau) \xi_{02}(\tau) \cos(n\theta) \sin(m\pi \zeta) \\
& - 2 \frac{\alpha m^2 n^2}{\pi^2 (9m^2 + \gamma^2)^2} \xi_{11}(\tau) \xi_{02}(\tau) \cos(n\theta) \sin(3m\pi \zeta) + \frac{1}{32} \frac{\alpha n^2}{m^2 \pi^2} \xi_{11}^2(\tau) \cos(2m\pi \zeta) \\
& - \frac{1}{32} \frac{\beta^4 h m^2 \pi^2}{n^2 \alpha^3} \xi_{11}^2(\tau) \cos(2n\theta)
\end{aligned} \tag{8}$$

Substituting Eq. (7) and Eq. (8) into Eq. (2) and applying the Galerkin method, a set of two non-linear differential equations of motion in terms of the modal amplitudes are obtained:

$$\begin{aligned}
16 \frac{\rho h^2 \omega_0^2}{\pi^2 E n m} \ddot{\xi}_{11}(\tau) + 8 \frac{h \omega_0}{E n m} \left[\frac{\beta_1}{\pi^2} + \frac{\beta_2 \pi^2}{L^4} (m^2 + \gamma^2)^2 \right] \dot{\xi}_{11}(\tau) \\
- 4 \frac{\alpha^3 n}{\pi^2} \left[\frac{8 m^3}{(m^2 + \gamma^2)^2} + \frac{1}{m} \right] \xi_{11}(\tau) \xi_{02}(\tau) + \frac{1}{2} \frac{\beta^4 \pi^2 (m^4 + \gamma^4)}{m n} \xi_{11}^3(\tau) \\
+ \left[8 \frac{\alpha^2 m^3}{\pi^2 n (m^2 + \gamma^2)^2} + \frac{2 \pi^2 \beta^4 (m^2 + \gamma^2)^2}{3 m n (1-\nu^2)} - 8 \frac{[\Gamma_0 + \Gamma_1 \cos(\Omega \tau)] \alpha \beta^2 m}{n \sqrt{3(1-\nu^2)}} \right] \xi_{11}(\tau) \\
+ 32 \frac{\alpha^4 n^3 m^3}{\pi^2} \left[\frac{1}{(9m^2 + \gamma^2)^2} + \frac{1}{(m^2 + \gamma^2)^2} \right] \xi_{11}(\tau) \xi_{02}^2(\tau) = 0
\end{aligned} \tag{9}$$

$$\begin{aligned}
32 \frac{\rho h^2 \omega_0^2}{\pi^2 E n m} \ddot{\xi}_{02}(\tau) + 16 \frac{h \omega_0}{E n} \left[\frac{\beta_1}{\pi^2 m} + 16 \frac{\pi^2 \beta_2 m^3}{L^4} \right] \dot{\xi}_{02}(\tau) \\
+ 32 \frac{\alpha^4 n^3 m^3}{\pi^2} \left[\frac{1}{(9m^2 + \gamma^2)^2} + \frac{1}{(m^2 + \gamma^2)^2} \right] \xi_{11}^2(\tau) \xi_{02}(\tau) \\
- 2 \frac{\alpha^3 n}{\pi^2} \left[\frac{8 m^3}{(m^2 + \gamma^2)^2} + \frac{1}{m} \right] \xi_{11}^2(\tau) \\
+ \left[16 \frac{\alpha^2}{\pi^2 m n} + \frac{64 \pi^2 \beta^4 m^3}{3 n (1-\nu^2)} - 64 \frac{[\Gamma_0 + \Gamma_1 \cos(\Omega \tau)] \alpha \beta^2 m}{n \sqrt{3(1-\nu^2)}} \right] \xi_{02}(\tau) = 0
\end{aligned} \tag{10}$$

3 NUMERICAL RESULTS

For the analysis the following geometric and physical shell parameters are used $R = 0.2$ m, $L = 0.4$ m, $h = 0.002$ m, $E = 210$ GPa, $\nu = 0.3$, $\rho = 7850$ kg/m³. The damping coefficients are, respectively, given by $\eta_1 = 0.0008$ and $\eta_2 = 0.0001$ (Pellicano e Amabili, 2003). For this shell geometry, the lowest natural frequency and critical load occur for $(m,n) = (1,5)$ (Gonçalves e Del Prado, 2005).

For the parametric stability analysis and escape from the pre-buckling well the previous knowledge of the post-critical path is obtained using the Newton-Raphson method. Figure 2

displays the post-critical path of the shell for modal amplitude ξ_{11} as a function of the static load parameter Γ_0 . It is possible to observe that the shell, after a critical load parameter ($\Gamma_0 = 1.0$), loses stability at an unstable symmetric bifurcation point. The post-critical path remains unstable up to a minimum value and, after this minimum, becomes stable. This non-linear softening behavior is typical for cylindrical shells.

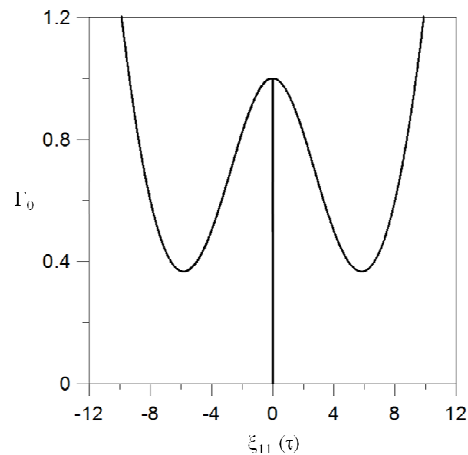


Figure 2: Post critical path for the shell under static axial load

Figure 3 shows the instability and permanent escape boundaries of the shell for different levels of the static load parameter in the (Γ_0, Ω) space. All curves are plotted with the same displacement and velocity initial conditions given as 1×10^{-4} . In Figures 3a-c the dotted horizontal lines represent the static critical load, $\Gamma_{CR} = \Gamma_0 + \Gamma_1$, meanwhile the vertical dotted line ($2\omega_p$) represents the valley which is associated to the principal parametric instability and the vertical dotted line (ω_p) represents the valley which is associated to the secondary instability region of the shell (direct resonance).

For initial conditions (Γ_0, Ω) under the parametric instability boundary, the cylindrical shell displays a trivial steady-state solution, for initial conditions (Γ_0, Ω) between the parametric instability and escape boundaries, the shell shows small amplitude vibrations in steady-state vibrations within the pre-buckling well. Finally, for initial conditions (Γ_0, Ω) above the escape boundary the shell will display large amplitude steady-state vibrations. This corresponds to escape from the pre-buckling well. The limits of the pre-buckling well are obtained from the post-critical path of the shell (Figure 2) and, for each loading level, it indicates a maximum amplitude vibrations.

Figure 3d displays the superposition of boundaries from Figures 3a-c. It is possible to observe that, increasing the static pre-loading parameter, Γ_0 , there is a reduction of the instability load amplitude, Γ_1 , for both parametric instability and permanent escape boundaries. The normalized frequency parameter, Ω^* , is obtained from the $\Omega / \omega_{p,\Gamma_0}$ ratio where ω_{p,Γ_0} represents the natural frequency of the loaded shell for each pre-loading static parameter, Γ_0 .

Figure 4 shows the time responses and its corresponding phase plane obtained for increasing values of the static pre-loading parameter equal to Γ_0 and frequency load parameter $\Omega = 1.20$. These figures describe the typical dynamic behavior defined by the parametric and permanent escape boundaries shown in Figure 3b.

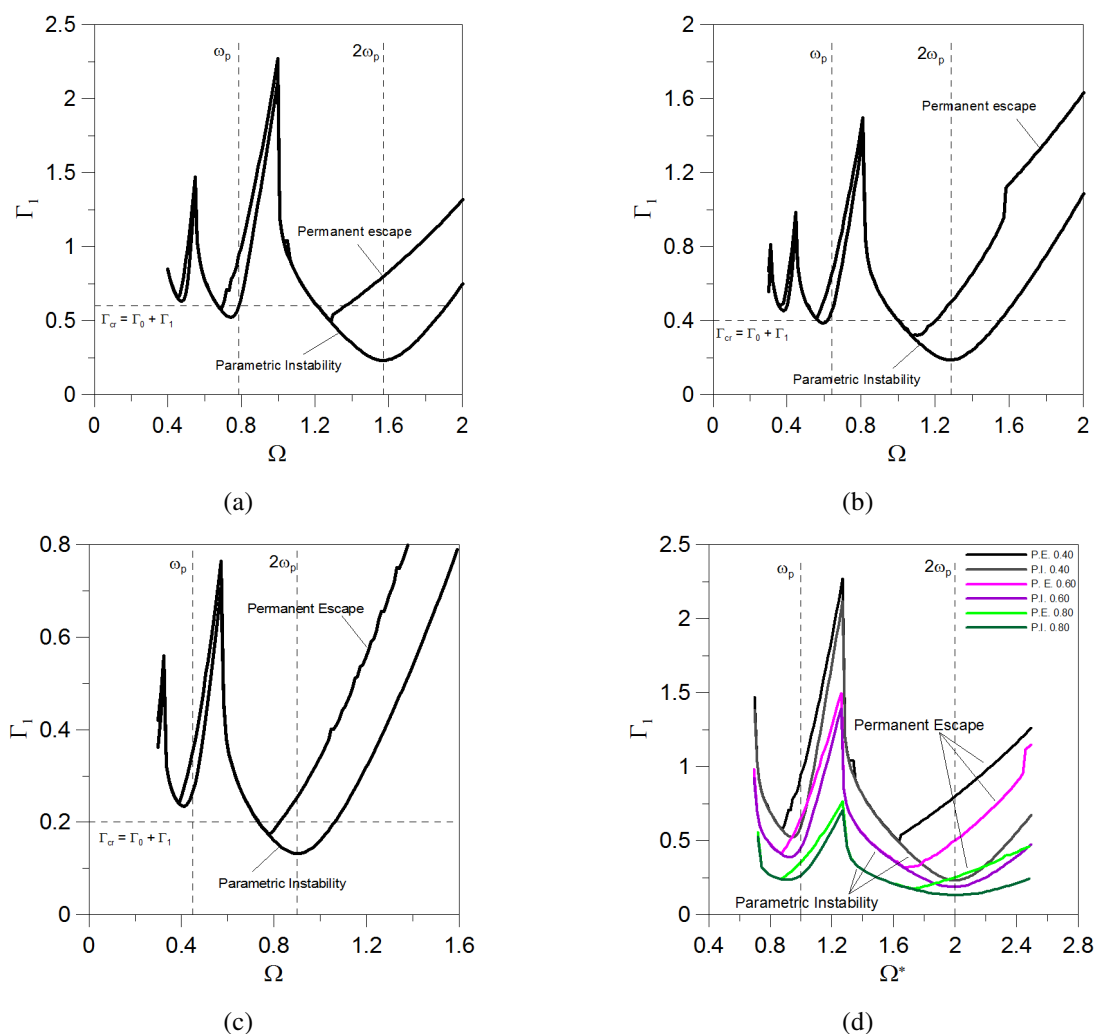


Figure 3: Parametric instability and permanent escape boundaries. (a) $\Gamma_0 = 0.40$. (b) $\Gamma_0 = 0.60$. (c) $\Gamma_0 = 0.80$. (d) Boundaries superposition. (P.E. – permanent escape and P.I. – parametric instability)

Figures 4a-b shows the time response and phase plane for a shell with parameters (Γ_1, Ω) below the parametric instability boundary. In this case the shell after an initial perturbation exhibits a response that converges to the trivial solution.

Figure 4c-d display the time response and phase plane for a shell with parameters (Γ_1, Ω) , between the parametric instability and escape boundaries. In this region, the shell vibrates with small amplitude oscillations within the pre-buckling well. Finally, Figures 4e-f show the time response and phase plane for a shell with parameters (Γ_1, Ω) above the permanent escape boundary and, in this case, the shell displays large amplitude vibrations (cross-well motions).

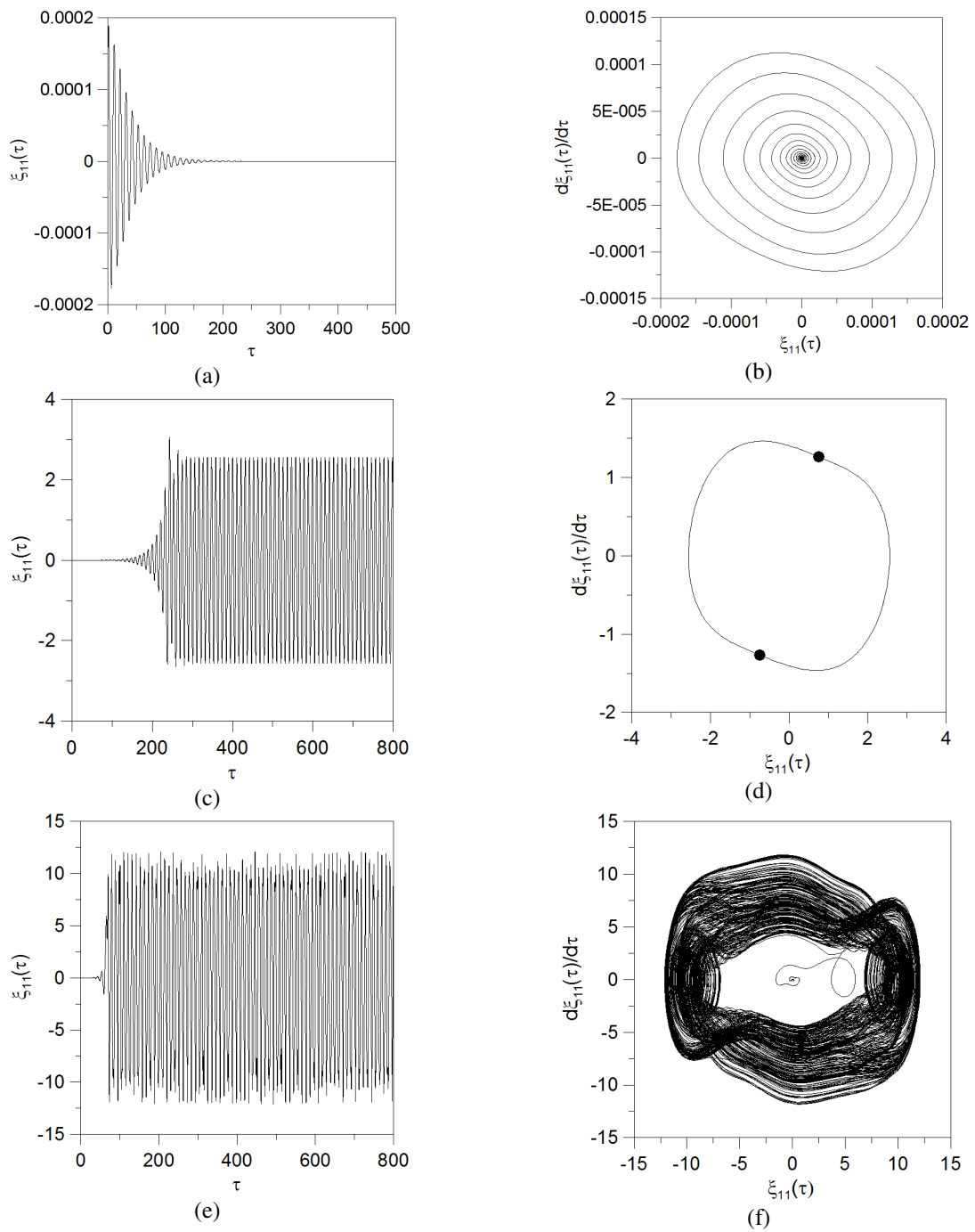


Figure 4: Time responses and phase planes for $\Omega = 1.20$. • - Fixed points obtained from the Poincare mapping.
 (a) Time response for $\Gamma_1 = 0.15$; (b) Phase plane for $\Gamma_1 = 0.15$; (c) Time response for $\Gamma_1 = 0.30$; (d) Phase plane for $\Gamma_1 = 0.30$; (e) Time response for $\Gamma_1 = 0.60$; (f) Phase plane for $\Gamma_1 = 0.60$

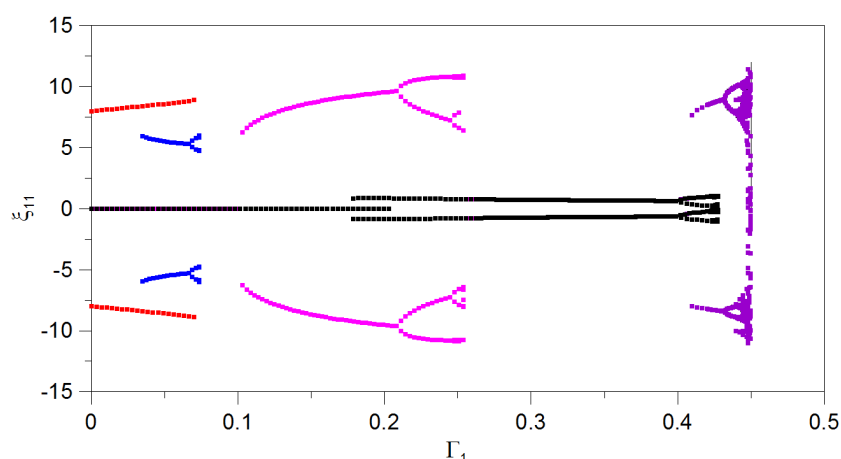


Figure 5: Sub-critical bifurcation diagram for $\Gamma_0 = 0.60$ and $\Omega = 1.20$. Principal instability region

Figure 5 displays a typical bifurcation diagram obtained for a static pre-loading parameter $\Gamma_0 = 0.60$, $\Omega = 1.20$ and increasing values of the load parameter Γ_1 . In this figure all stable solutions are displayed in both pre-buckling (black dots) and post-buckling wells (red and blue dots). From this bifurcation diagram it is possible to evaluate the evolution of the shell stable permanent solutions for variation of the load parameter as well as the bifurcations associated to the parametric instability and escape boundaries. This bifurcation diagram is typical of the descending branch in the principal instability region where a sub-critical bifurcation occurs. This means that, after a certain critical point, the stable solution in the pre-buckling well jumps to a stable periodic solution with period $2T$.

Figure 6 shows the basins of attraction plotted for different Γ_1 values associated with the bifurcation diagram shown in Figure 5. In these basins of attraction and, for each initial condition in the plane $\xi_{11} \times d\xi_{11}/d\tau$, the attractors of all stable permanent solution responses were obtained.

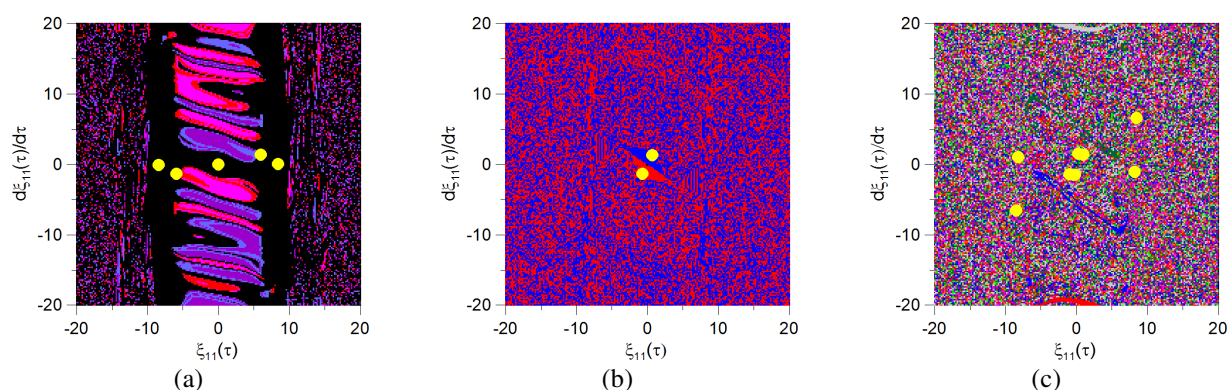


Figure 6: Cross-section of basins of attraction for $\Gamma_0 = 0.60$ and $\Omega = 1.20$. (a) $\Gamma_1 = 0.035$; (b) $\Gamma_1 = 0.35$; (c) $\Gamma_1 = 0.42$

The response of the cylindrical shell is defined within a tetra-dimensional space and, to build the basins of attraction cross-sections shown in Figure 6 it was considered that $\xi_{02} = d\xi_{02}/d\tau = 1 \times 10^{-4}$. The black region represents the initial conditions that converge to the trivial solution in the pre-buckling well and the red and blue regions represent solutions that converge to small amplitude oscillations within the pre-buckling well. Other colors represent

solutions that converge to attractors out from the pre-buckling well. In this figure, yellow points represent the fixed points from the Poincare mapping.

Figure 7 displays the integrity factor of the pre-buckling well solutions for increasing values of Γ_1 . The integrity factor is the maximum radius of a hyper-sphere centered in a given attractor belonging entirely to the basins of attraction associated with the pre-buckling well (yellow dots of Figure 6) and gives a local measure of the compact basin around the attractor (Soliman and Thompson, 1989; Gonçalves et al. 2010). It is called by Thompson and co-workers Local Integrity Factor (LIM). In Figure 7 it possible to observe that for certain values of Γ_1 the integrity factor grows indefinitely, this is due to the fact that no stable solution exists out of the pre-buckling well, as shown in Figure 5 (Gonçalves et al. 2010).

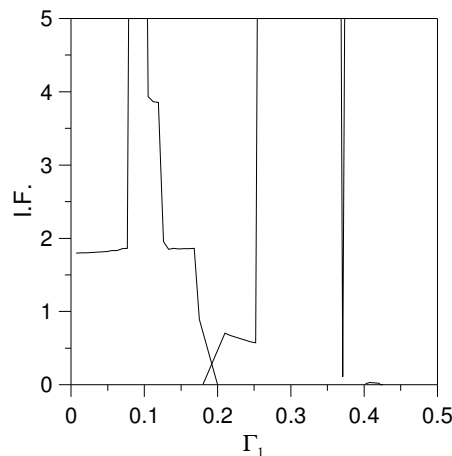


Figure 7: Integrity factor for load parameter variation ($\Gamma_0 = 0.60$ and $\Omega = 1.20$)

To verify the influence of the static pre-loading parameter, Γ_0 , on the integrity factor, Figures 8 and 9 show several bifurcation diagrams for the same instability region.

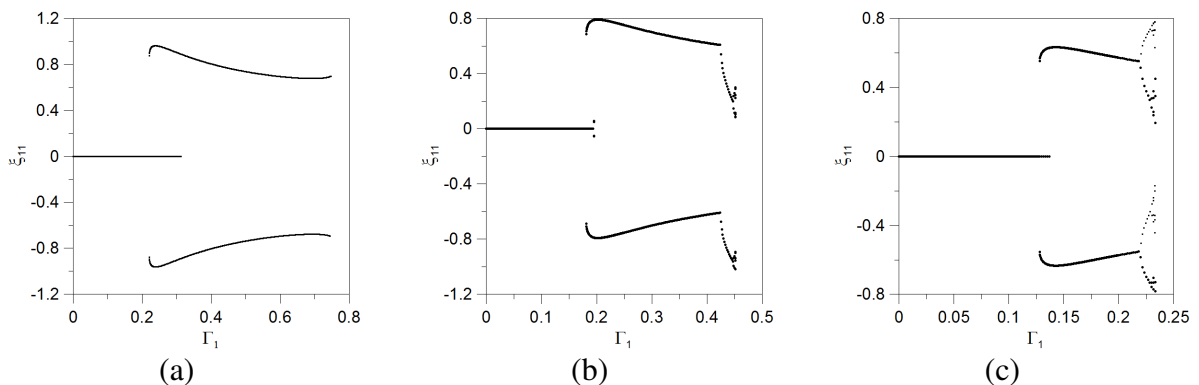


Figure 8: Bifurcation diagrams for $\Omega^* = 1.90$. (a) $\Gamma_0 = 0.40$; (b) $\Gamma_0 = 0.60$; (c) $\Gamma_0 = 0.80$

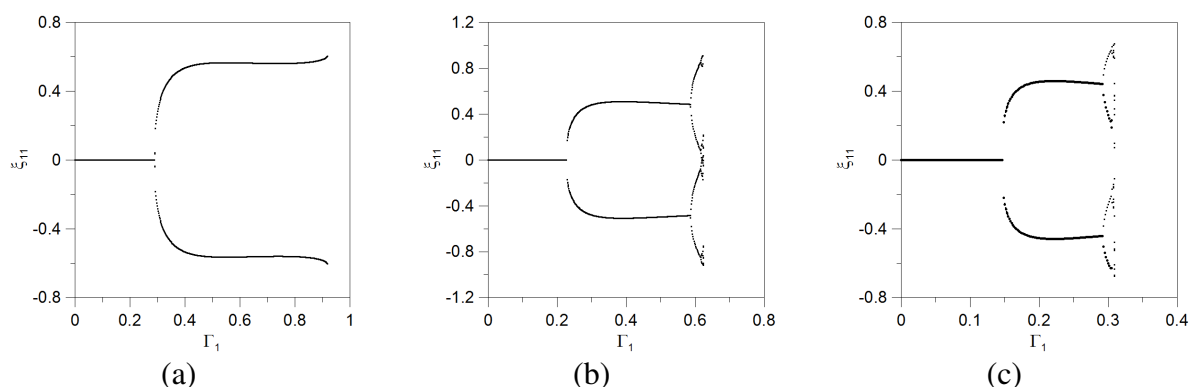


Figure 9: Bifurcation diagrams for $\Omega^* = 2.10$. (a) $\Gamma_0 = 0.40$; (b) $\Gamma_0 = 0.60$; (c) $\Gamma_0 = 0.80$

The bifurcations diagrams in Figures 8 and 9 are characteristics to the principal instability region. The diagrams in Figure 8 are characteristics to the descending branch (sub-critical bifurcations) and the diagrams in Figure 9 are characteristics to the ascending branch (super-critical bifurcations). It is possible to observe that the variation of the static pre-loading parameter does not modify the loss of stability mechanism of the shell but the amplitude of Γ_1 that leads to bifurcation or escape is reduced as Γ_0 increases, as shown in Figure 3d.

Figures 10 and 11 display the variation of the integrity factor plotted for the stable pre-buckling well solutions for, respectively, $\Omega^* = 1.90$ (Figure 8) and $\Omega^* = 2.10$ (Figure 9) and three different levels of Γ_0 .

Tables 1 and 2 show some values of the integrity factor obtained from Figures 10 and 11. As can be observed, for certain values of Γ_1 , the integrity factor grows indefinitely due to the lack of stable solutions out from the pre-buckling well, as shown in Figure 7. For $\Gamma_0 = 0.80$ the integrity factor can be is always determined, meaning that there exist a family of solutions out from the pre-buckling well that limits the radius of the hyper-sphere.

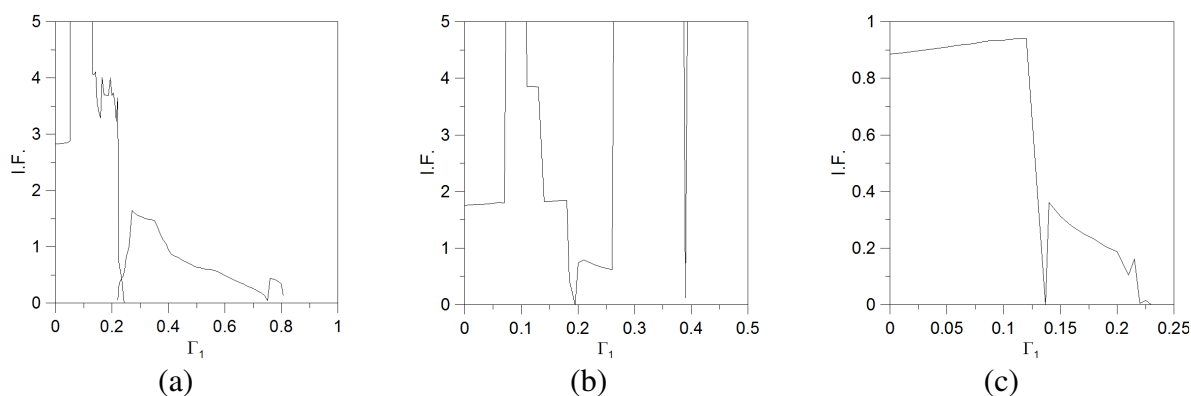


Figure 10: Variation of the integrity factor for $\Omega^* = 1.90$. (a) $\Gamma_0 = 0.40$; (a) $\Gamma_0 = 0.60$; (a) $\Gamma_0 = 0.80$

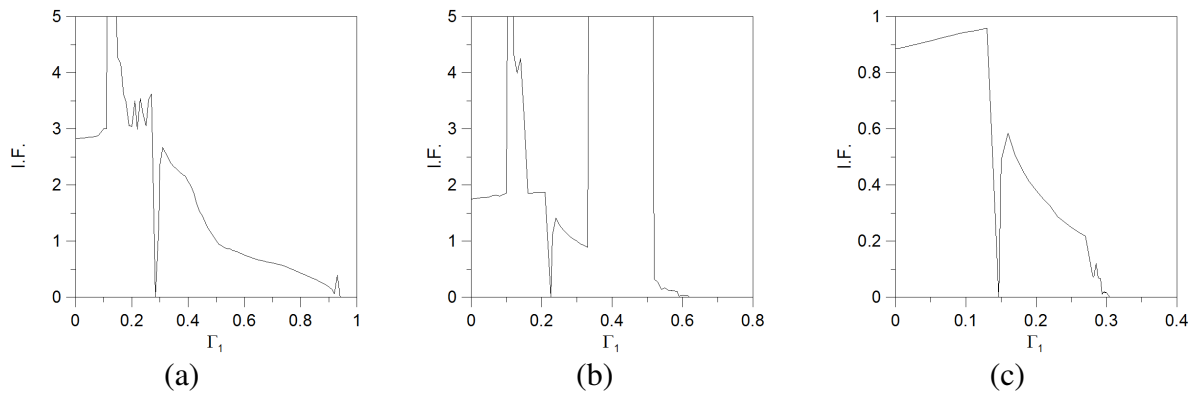


Figure 11: Variation of the integrity factor for $\Omega^* = 2.10$. (a) $\Gamma_0 = 0.40$; (b) $\Gamma_0 = 0.60$; (c) $\Gamma_0 = 0.80$

	$\Gamma_0 = 0.40$	$\Gamma_0 = 0.60$	$\Gamma_0 = 0.80$
$\Gamma_1 = 0.03$	2.839	1.773	0.900
$\Gamma_1 = 0.06$	-	1.801	0.917
$\Gamma_1 = 0.10$	-	-	0.935
$\Gamma_1 = 0.12$	-	3.860	0.942

Table 1: Integrity factors in the fundamental solution ($\Omega^* = 1.90$)

	$\Gamma_0 = 0.40$	$\Gamma_0 = 0.60$	$\Gamma_0 = 0.80$
$\Gamma_1 = 0.05$	2.852	1.789	0.915
$\Gamma_1 = 0.11$	3.006	-	0.949
$\Gamma_1 = 0.12$	-	4.328	0.954
$\Gamma_1 = 0.14$	5.417	4.252	0.385

Table 2: Integrity factors in the fundamental solution ($\Omega^* = 2.10$)

4 CONCLUDING REMARKS

In this work, the Donnell shallow shell theory is used to study the non-linear dynamic behavior of simply supported cylindrical shells subjected to axial harmonic loads. A modal expansion with two degrees of freedom is used to describe the lateral displacement and a set of non-linear equilibrium equations are obtained by using the Galerkin method. For different levels of pre-static loading, the integrity factor of the shell is obtained. This factor can be associated to the degree of safety of the structure when subjected to dynamic excitations. The obtained results show that for certain values of the static pre-loading parameter the integrity factor can show very different values indicating higher or lower level of safety in the presence of external perturbations.

REFERENCES

- Gonçalves, P.B. and Del Prado, Z.J.G.N., Low-dimensional Galerkin models for nonlinear vibration and instability analysis of cylindrical shells. *Nonlinear Dynamics*, 41:129-145, 2005.
- Gonçalves, P.B., Silva, F.M.A., and Del Prado, Z.J.G.N., Global stability analysis of parametrically excited cylindrical shells through the evolution of basin boundaries. *Nonlinear Dynamics*, 50:121-145, 2007a.
- Gonçalves, P.B., Silva, F.M.A., and Del Prado, Z.J.G.N., Transient and steady state stability of cylindrical shells under harmonic axial loads. *International Journal of Non-linear Mechanics*, 42:58-70, 2007b.
- Gonçalves, P.B., Silva, F.M.A., and Del Prado, Z.J.G.N., Low dimensional models for the nonlinear vibration analysis of cylindrical shells based on a perturbation procedure and proper orthogonal decomposition. *Journal of Sound and Vibration*, 315:641-663, 2008.
- Gonçalves, P.B., Silva, F.M.A., Rega, G. and Lenci, S., Global dynamics and integrity of a two-dof model of a parametrically excited cylindrical shell. *Nonlinear Dynamics*. In Press (<http://dx.doi.org/10.1007/s11071-010-9785-4>):1-22, 2010.
- Grebogi, C., Ott, E. and Yorke, J.A., Basin boundary metamorphoses: changes in accessible boundary orbits. *Physica D*, 24:243-262, 1987.
- Lansbury, A.N., Thompson, J.M.T. and Stewart, H.B., Basin erosion in the twin-well Duffing oscillator: two distinct bifurcation scenarios. *International Journal of Bifurcation Chaos*, 2:505-532, 1992.
- McDonald, S.W., Grebogi, C., Ott, E. and Yorke, J.A., Fractal basin boundaries. *Physica D*, 17:125-153, 1985.
- Pellicano, F. and Amabili, M., Stability and vibration of empty and fluid-filled circular cylindrical shells under static and periodic axial loads. *International Journal of Solids and Structures*, 40:3229-3251, 2003.
- Rega, G., Lenci, S., Identifying, evaluating, and controlling dynamical integrity measures in non-linear mechanical oscillators. *Nonlinear Analysis*, 63:902-914, 2005.
- Silva, F.M.A., *Low dimensional models for nonlinear vibration analysis and stability of cylindrical shells*. D. Sc. Thesis, Catholic University of Rio de Janeiro, PUC-Rio, Rio de Janeiro, Brazil, 2008.
- Soliman, M.S., Jumps to resonance: long chaotic transients unpredictable outcome and the probability of reestablishment. *Journal of Applied Mechanics*, 60:669-676, 1993.
- Soliman, M.S. and Thompson, J.M.T., Integrity measures quantifying the erosion of smooth and fractal basins of attraction. *Journal of Sound and Vibration*, 135:453-475, 1989.
- Soliman, M.S. and Thompson, J.M.T., Basin organization prior to a tangled saddle-node bifurcation. *International Journal of Bifurcation and Chaos*, 1:107-118, 1991.
- Thompson, J.M.T., Chaotic phenomena triggering the escape from a potential well. *Proceedings of the Royal Society A*, 421:195-225, 1989.
- Thompson, J.M.T. and Soliman, M.S., Indeterminate jumps to resonance from a tangled saddle-node bifurcation, *Proceedings of the Royal Society A*, 432:101-111, 1991.